Matrix Isolation Infrared Observation of $H_xSi(N_2)_y$ ($x = 0, 1, 2$ and $y = 1, 2$) Transient Species Using a 121-nm Vacuum Ultraviolet Photolysis Source

Jay C. Amicangelo,* Christopher T. Dine, Daniel G. Irwin, Cynthia J. Lee, Natalie C. Romano, and Nancy L. Saxton

School of Science, Penn State Erie, The Behrend College, 4205 College Drive, Erie, Pennsylvania 16563-0203

Received: August 11, 2007; In Final Form: January 3, 2008

Vacuum ultraviolet photolysis (121.6 nm) of silane in a nitrogen matrix at 12 K leads to the observation of several transient species, which have been characterized using Fourier transform infrared spectroscopy. Four transient species containing silicon and nitrogen have been observed (SiN_2, $Si(N_2)_2$, $HSiN_2$, and H_2SiN_2), and one transient species containing only silicon and hydrogen has been observed. The assignment of the infrared bands due to each of these species is accomplished by performing isotopic substitution experiments (SiD_4, $^{15}N_2$, and mixtures with SiH_4 and $^{14}N_2$), matrix annealing experiments, UV−visible photolysis experiments, by comparison with previous experimental matrix isolation frequencies, where available, and for $HSiN_2$ and H_2SiN_2 by comparison to B3LYP/aug-cc-pVTZ-calculated vibrational frequencies. The observation and infrared assignment of the $HSiN_2$ and H_2SiN_2 molecules in these experiments is significant in that $HSiN_2$ has not been previously reported in the matrix isolation literature, and H_2SiN_2 has only been reported once previously by a different route of formation. The energetics of the overall formation pathways for the molecules observed in these experiments is discussed using B3LYP/aug-cc-pVTZ calculations.

Introduction

Silane (SiH_4) is an important and widely used material in the semiconductor and electronics industry in the manufacture of thin films of silicon, silicon dioxide, silicon nitride, and any other material requiring silicon.[1] Typically the thin films are deposited onto a substrate by the use of chemical vapor deposition (CVD) processing, whereby gas-phase reagents are decomposed by some means of energy input into solid-phase inorganic materials.[2,3] The most common method used in CVD for decomposing the reagents is high-temperature pyrolysis, known as thermal CVD, but the use of high-frequency plasmas, known as plasma-enhanced CVD, and high-energy photolysis, known as photoassisted CVD, have also come into use. Photoassisted CVD has several advantages over thermal or plasma-enhanced CVD in the use of lower substrate temperatures, lower amount of damage to the substrate and deposited layers, and the potential for minimizing side reactions. To fully realize these advantages, a complete understanding of the mechanism of photoassisted CVD is needed, including dominant fragmentation pathways and reaction intermediates in various environments and conditions.[4]

When silane is used as the reagent for photoassisted CVD, the wavelengths required are in the low ultraviolet or vacuum-ultraviolet (VUV) region. The VUV photodissociation of SiH_4 in the gas phase has been studied previously by several researchers,[5−9] and the primary photoproducts that were detected were silicon atoms, the SiH radical, and atomic and molecular hydrogen. This is in contrast to the thermal CVD process using SiH_4, in which the dominant intermediate is thought to be SiH_2.[10] Part of the ambiguity in the gas-phase photodissociation studies is that, due to the very low pressures used, even if higher silicon hydrides, such as SiH_3 or SiH_2, were being formed, in the nearly collision free environment the excess excitation energy would most likely cause further, rapid dissociations and therefore hamper the efforts to directly observe these species.

The matrix isolation spectroscopy technique can help in this regard, given that one of its primary uses is in the characterization of transient and reactive species. There has only been one previous matrix isolation study of the VUV photodissociation of SiH_4 by Jacox and Milligan.[11] In this study, SiH_4 was deposited in a 12 K argon matrix while being simultaneously photolyzed with 121.6-nm photons, and the resulting products were examined using infrared and UV−vis spectroscopies. Although several of the initial infrared assignments made in this study proved to ultimately be incorrect,[12−15] a re-examination of their infrared spectra seem to indicate that the transient species observed were SiH_3, SiH_2, SiH, and Si_2 (identified from the UV−vis spectra). In their study of the photodissociation of SiH_4 in argon matrices, Milligan and Jacox also reported performing VUV photodissociation experiments with SiH_4 in 12 K nitrogen matrices and observed several previously unidentified infrared bands at 2026, 2012, 1755, and 1738 cm^{-1} in these experiments.[11] They speculated that the peaks they observed might be due to species of the type SiH_xN_2; however, they did not fully analyze the nitrogen matrix infrared spectra and therefore never made definitive assignments for these bands. In this work, the products of the VUV photolysis of SiH_4 in a 12 K nitrogen matrix is reinvestigated using Fourier transform infrared spectroscopy. The identification and assignment of the infrared bands of the transient species formed in the current experiments was accomplished by performing isotopic substitution experiments (SiD_4, $^{15}N_2$, and mixtures with SiH_4 and $^{14}N_2$), matrix annealing experiments, UV−vis photolysis experiments, by comparison with previous experimental matrix isolation frequencies, where available, and for two of the transient species, by comparison to B3LYP/aug-cc-pVTZ-calculated vibrational frequencies.

* To whom correspondence should be addressed. E-mail: jca11@psu.edu. Phone: (814) 898-6334. Fax: (814) 898-6213.

10.1021/jp076466m CCC: $40.75 © 2008 American Chemical Society
Published on Web 02/28/2008

Experimental and Theoretical Methods

The details of the matrix isolation apparatus used in these experiments have been described previously.[16] In the current experiments, 1−2% mixtures of SiH_4 (Scott Specialty Gases, 99.9999%) in N_2 (Praxair, 99.9995%) were deposited onto a CsI window at 12 K for 3−4 h at a rate of 2−4 mmol/hour while simultaneously photolyzing the mixture with the 121.6-nm Lyman-α radiation from a hydrogen resonance lamp (Opthos). This lamp consists of a quartz tube body that is sealed with a MgF_2 window and filled with a mixture that is 10% hydrogen and 90% argon at approximately 1 Torr. The gas is excited using an Evenson-Broida microwave discharge cavity[17] (Opthos) powered by a 300-W microwave power supply (Sairem, 2540 MHz) typically operating at 40 W. Infrared spectra were recorded on a Nicolet Nexus 670 Fourier-transform infrared spectrometer at 0.5 or 1.0 cm^{-1} resolution, with at least 128 or 256 scans co-added, respectively. In several experiments, the deposited matrices were annealed to temperatures between 20−30 K for approximately 30 min, followed by recooling to 12 K and rescanning of the spectra. In addition, several deposits were subjected to UV−visible photolysis using the full output (UV plus visible) or long pass filtered output (visible only; 400 nm cutoff) of a 200-W Hg−Xe arc lamp (Thermo-Oriel). Isotopic experiments were also performed utilizing SiD_4 (Spectra Gases, 98% D) and $^{15}N_2$ (Cambridge Isotope Laboratories, 98+% ^{15}N) and mixtures of these isotopic gases with SiH_4 and $^{14}N_2$.

For two of the transient species observed in the current experiments ($HSiN_2$ and H_2SiN_2) and one potential transient species (H_3SiN_2), density functional theory calculations using the B3LYP hybrid functional[18,19] and the aug-cc-pVTZ basis set[20−22] were performed to predict equilibrium geometries and vibrational frequencies. The geometries were fully optimized using tight convergence criteria, and vibrational frequencies were calculated using analytical second derivatives. To aid in the discussion of the energetic of the possible formation pathways of all of the transient species observed in the current experiments, geometry optimizations and frequency analyses were also performed for all other species at the B3LYP/aug-cc-pVTZ level and zero-point energy corrected interaction energies for the various possible formation pathways were calculated. All calculations used the Gaussian 03 suite of programs.[23]

Results and Discussion

Infrared Spectra. A series of experiments were performed in which samples of SiH_4 in N_2 are deposited onto a CsI window at 12 K while simultaneously being photolyzed with the 121-nm VUV radiation from a hydrogen resonance lamp. Typical infrared spectra of a photolyzed vs unphotolyzed SiH_4 in N_2 sample at 12 K are displayed in Figure 1, and as can be seen, there are several new absorptions that appear upon VUV photolysis of the sample. The absorptions at 836.8 and 939.1 cm^{-1} are readily assigned to the stable molecule Si_2H_6.[11,13,15] There is also a weak, broad absorption at 873.2 cm^{-1} and a sharp band at 876.3 cm^{-1} that grows in upon annealing to 30 K that are close in frequency to bands that have been assigned in previous matrix isolation studies to higher saturated silicon hydrides, such as Si_3H_8.[13,15] A broad band is observed at 1100.4 cm^{-1} that is in very good agreement with several previously reported experimental matrix isolation assignments of the antisymmetric Si−H−Si stretching mode for a dibridged Si_2H_2 molecule in neon and argon matrices,[15,24,25] and on the basis of this agreement, we assign this peak as such. Of the remaining absorptions, the bands between 2300 and 1700 cm^{-1} are assigned to transient species containing silicon and nitrogen, and the specific assignments are made on the basis of annealing experiments, UV−vis photolysis experiments, isotopic experiments, previous experimental matrix isolation studies where available, and density functional theory calculations in two cases.

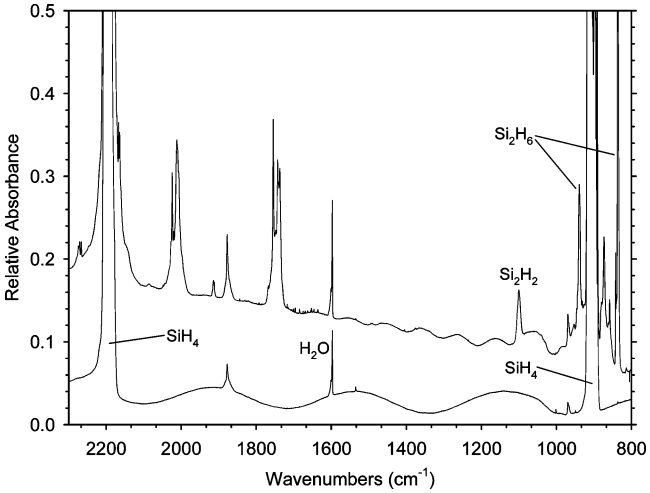

Figure 1. Infrared spectra in the 2300−800 cm^{-1} region for deposition of 1% SiH_4 in nitrogen at 12 K for 2 h (lower) and deposition of 1% SiH_4 in nitrogen at 12 K for 4 h with simultaneous photolysis by a 121.6-nm hydrogen resonance lamp (upper).

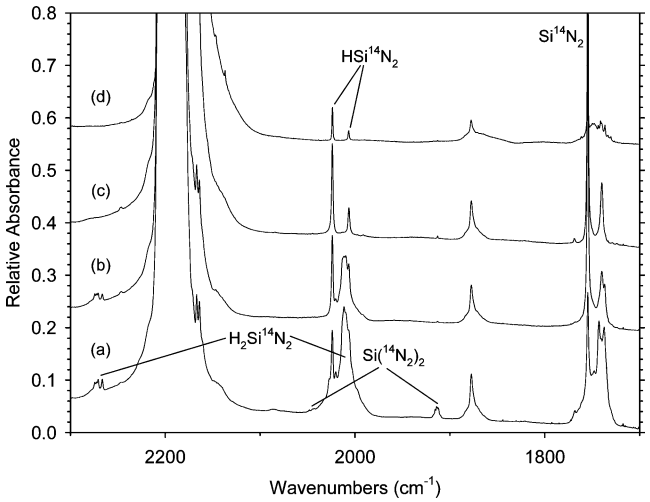

Figure 2. Infrared spectra in the 2300−1700 cm^{-1} region for 1% SiH_4 in $^{14}N_2$ deposited at 12 K (a) with simultaneous 121.6-nm hydrogen resonance lamp photolysis for 4 h, (b) after 400−900-nm irradiation for 30 min, (c) after 200−900-nm irradiation for 30 min, and (d) after annealing to 30 K for 30 min.

The sequence of experiments that proved to be the most useful in making the assignments for the Si- and N_2-containing species was to follow the initial VUV photolysis deposition by filtered Hg−Xe lamp irradiation ($\lambda > 400$ nm) of the sample for 30 min, which was then followed by unfiltered Hg−Xe lamp irradiation ($\lambda > 200$ nm) for 30 min, and finally 30 K annealing for 30 min. Spectra resulting from the experiments with $SiH_4 + {}^{14}N_2$, $SiD_4 + {}^{14}N_2$, $SiH_4 + {}^{15}N_2$, $SiD_4 + {}^{15}N_2$, $SiH_4 + {}^{14}N_2 + {}^{15}N_2$, and $SiD_4 + {}^{14}N_2 + {}^{15}N_2$ mixtures are displayed in Figures 2−7, respectively, and the absorption bands for the major trapping sites (assigned below) observed for the silicon- and nitrogen-containing transient species are listed in Table 1. For each of these mixtures, experiments were also performed in which, after the initial VUV photolysis deposition, the sample was annealed to 20, 25, and 30 K for 30 min at each temperature and these spectra are given in the Supporting Information. For

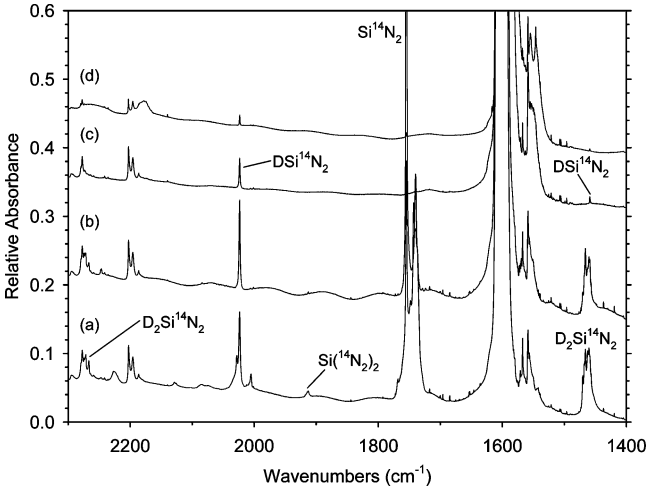

Figure 3. Infrared spectra in the 2300−1400 cm^{-1} region for 1% SiD_4 in $^{14}N_2$ deposited at 12 K (a) with simultaneous 121.6-nm hydrogen resonance lamp photolysis for 4 h, (b) after 400−900-nm irradiation for 30 min, (c) after 200−900-nm irradiation for 30 min, and (d) after annealing to 30 K for 30 min.

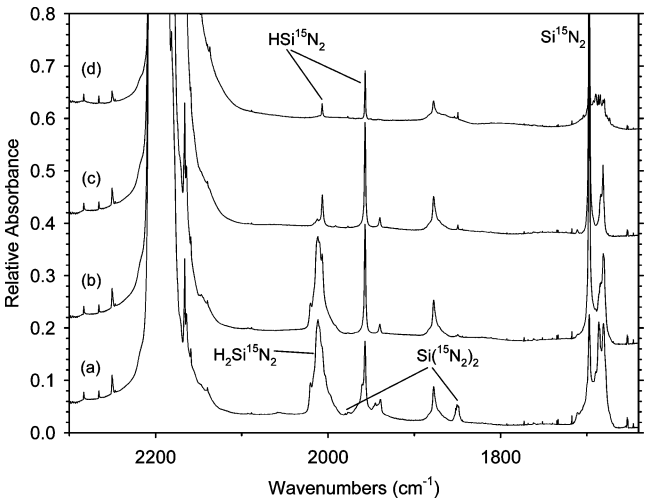

Figure 4. Infrared spectra in the 2300−1640 cm^{-1} region for 1% SiH_4 in $^{15}N_2$ deposited at 12 K (a) with simultaneous 121.6-nm hydrogen resonance lamp photolysis for 4 h, (b) after 400−900-nm irradiation for 30 min, (c) after 200−9000-nm irradiation for 30 min, and (d) after annealing to 30 K for 30 min.

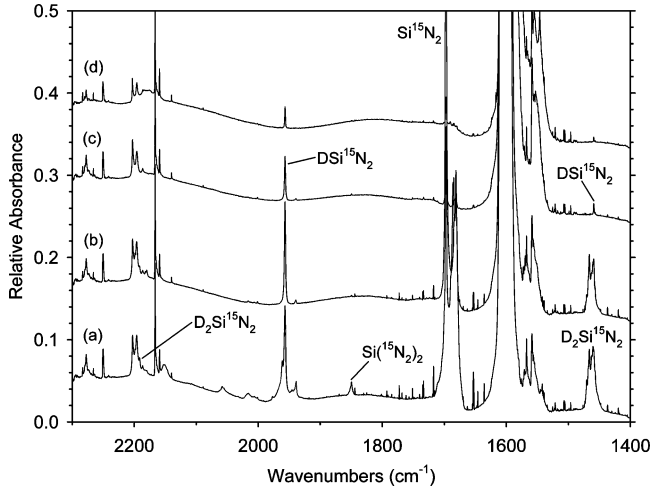

Figure 5. Infrared spectra in the 2300−1400 cm^{-1} region for 2% SiD_4 in $^{15}N_2$ deposited at 12 K (a) with simultaneous 121.6-nm hydrogen resonance lamp photolysis for 4 h, (b) after 400−900-nm irradiation for 30 min, (c) after 200−900-nm irradiation for 30 min, and (d) after annealing to 30 K for 30 min.

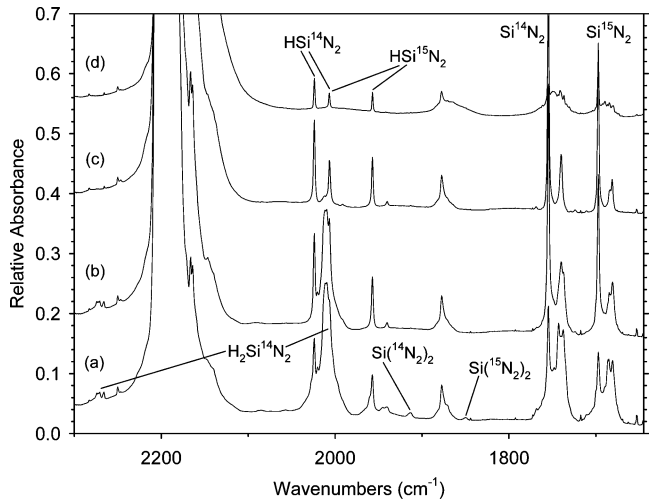

Figure 6. Infrared spectra in the 2300−1645 cm^{-1} region for 1% SiH_4 in a 1.5:1 $^{14}N_2$:$^{15}N_2$ mixture deposited at 12 K (a) with simultaneous 121.6-nm hydrogen resonance lamp photolysis for 4 h, (b) after 400−900-nm irradiation for 30 min, (c) after 200−900-nm irradiation for 30 min, and (d) after annealing to 30 K for 30 min.

the assignment of two of the Si and N_2 containing species, the progressive annealing experiments proved to be crucial, and portions of these spectra for the SiH_4 + $^{14}N_2$, SiD_4 + $^{14}N_2$, SiH_4 + $^{15}N_2$, and SiD_4 + $^{15}N_2$ experiments are displayed in Figure 8. It was also determined that these same two species possessed Si−H vibrations, and therefore mixed SiH_4 + SiD_4 + $^{14}N_2$ experiments were performed, and expanded portions of the spectra resulting from these experiments are displayed in Figure 9.

Theoretical Calculations. Several of the species observed in these experiments have been theoretically characterized previously using various ab initio and density functional theory methods.[25−36] For the $HSiN_2$ molecule, the only previous theoretical study was the work of Ornellas and Iwata, in which they examined the [H, Si, N, N] potential energy surface at the Hartree−Fock (HF), second-order Møller−Plesset (MP2), and coupled cluster with single, double, and perturbative triple excitation (CCSD(T)) levels; however, it was found that only the CCSD(T) method predicted thermodynamic stability for the $HSiN_2$ isomer.[33] Similar conclusions have been reached regarding the failure of conventional ab initio methods to properly describe the bonding and vibrational frequencies of the SiN_2 molecule as well.[26−28,30−32] Maier and co-workers have performed a fairly extensive set of theoretical calculations, in conjunction with their experimental work, for a wide range of silicon-, nitrogen-, and hydrogen-containing transient species, including several observed in these experiments, using density functional theory[35,36] and have shown that the B3LYP hybrid functional is capable of adequately describing the bonding stability and vibrational frequencies of these species. Therefore, density functional theory calculations using the B3LYP hybrid functional have been performed for the $HSiN_2$ molecule as well as for the H_2SiN_2 and H_3SiN_2 molecules. In this work, we have chosen to use the aug-cc-pVTZ basis set because it has been shown to be useful in characterizing the energetics of weak complexes.[37−43] The optimized structures of these three molecules are shown in Chart 1, and the calculated vibrational frequencies and intensities of each vibrational mode are listed in Table 2.

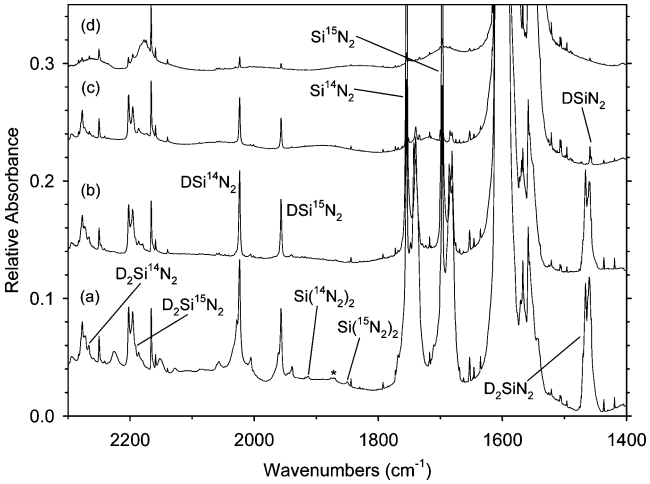

Figure 7. Infrared spectra in the 2300−1400 cm^{-1} region for 1% SiD_4 in a 1:1 $^{14}N_2$:$^{15}N_2$ mixture deposited at 12 K (a) with simultaneous 121.6-nm hydrogen resonance lamp photolysis for 4 h, (b) after 400−900-nm irradiation for 30 min, (c) after 200−900-nm irradiation for 30 min, and (d) after annealing to 30 K for 30 min. The peaks marked with an asterisk in panel a are due to the mixed isotopomer $^{14}N_2$−Si−$^{15}N_2$.

TABLE 1: Infrared Absorptions (cm^{-1}) for the Si- and N_2-Containing Species Observed in the VUV Photolysis of SiH_4 in Nitrogen Matrices at 12 K[a]

$SiH_4 + {}^{14}N_2$	$SiD_4 + {}^{14}N_2$	$SiH_4 + {}^{15}N_2$	$SiD_4 + {}^{15}N_2$	assignment
2274.2	2274.4		2198.6	H_2SiN_2, ν (N−N)
2044.5	2044.8	1977.0	1977.1	$Si(N_2)_2$, ν_s (N−N)
2023.9	2023.5	1957.1	1956.8	$HSiN_2$, ν (N−N)
2013.6[b]	1466.2[c]	2013.8[d]	1466.3[e]	H_2SiN_2, ν_{as} (Si−H)
2009.4[b]	1460.4[c]	2009.5[d]	1460.3[e]	H_2SiN_2, ν_s (Si−H)
2006.6[b]	1458.9[c]	2006.8[d]	1458.9[e]	$HSiN_2$, ν (Si−H)
1913.0	1912.9	1849.5	1849.5	$Si(N_2)_2$, ν_{as} (N−N)
1754.5	1754.6	1697.1	1697.1	SiN_2, ν (N−N)
813.7		810.8	627.8	$HSiN_2$, δ (H−Si−N)

[a] Only the peaks for the major trapping sites are listed in the table. [b] Obtained from the VUV-photolyzed $SiH_4 + {}^{14}N_2$ sample after annealing to 25 K for 30 min. [c] Obtained from the VUV-photolyzed $SiD_4 + {}^{14}N_2$ sample after annealing to 25 K for 30 min. [d] Obtained from the VUV-photolyzed $SiH_4 + {}^{15}N_2$ sample after annealing to 25 K for 30 min. [e] Obtained from the VUV-photolyzed $SiD_4 + {}^{15}N_2$ sample after annealing to 25 K for 30 min.

H_2SiN_2. The broad series of bands in the range of 2020−2009 cm^{-1} (Figure 2) are found to shift to the range 1471−1456 cm^{-1} with SiD_4 (Figures 3 and 5) and not to shift with $^{15}N_2$ (Figure 4), indicating that these vibrations involve hydrogen and not nitrogen. The average isotopic H/D ratio of several of these bands is found to be 1.3748, which is very close to the isotopic ratio of diatomic SiH/SiD in a 4 K argon matrix (1.3752),[15] suggesting that these bands are due to Si−H stretching modes. A weak series of bands between 2275−2266 cm^{-1} are found to track with the Hg−Xe lamp photolysis and annealing behavior of the 2020−2009 cm^{-1} bands, suggesting that these bands may belong to the same molecule as the 2020−2009 cm^{-1} bands. The 2275−2266 cm^{-1} bands do not shift with the use of SiD_4 but do shift with the use of $^{15}N_2$ indicating that these modes involve nitrogen and not hydrogen. Unfortunately, due to the presence of the intense SiH_4 antisymmetric stretching band near 2200 cm^{-1}, the shifted positions of these bands in the $SiH_4 + {}^{15}N_2$ experiment could not be determined. However, in the $SiD_4 + {}^{15}N_2$ experiment (Figure 5), the SiD_4 antisymmetric stretching band occurs near 1600 cm^{-1}, and distinct peaks between 2199−2191 cm^{-1} were observed for these bands after subtraction of the residual SiH_4 peaks (shown in Figure 10a). The average $^{14}N/^{15}N$ isotopic ratio of these bands is 1.0343, which is very close to isotopic ratio of diatomic N_2 in a 12 K nitrogen matrix (1.0345),[16] suggesting that these bands are due an N−N stretch of a dinitrogen species. In the $SiD_4 + {}^{14}N_2 + {}^{15}N_2$ experiment (Figure 7), only the pure isotopic counterparts were observed in the $SiD_4 + {}^{14}N_2 + {}^{15}N_2$ mixed isotope experiment, which suggests that only a single N_2 subunit is associated with this vibrational mode.

Maier and co-workers[36] observed a series of bands between 2274−2266, 2018−2013, and 2012−2009 cm^{-1} in a study in which $H_2Si(N_3)_2$ or $(CH_3)_3SiSiH_3$ was photolyzed (254 nm) or flash pyrolyzed (700 °C) in a nitrogen matrix at 10 K. These researchers also performed isotopic labeling experiments with $D_2Si(N_3)_2$, $(CH_3)_3SiSiD_3$, and $^{15}N_2$ in order to fully assign these infrared bands. The combination of $D_2Si(N_3)_2$ or $(CH_3)_3SiSiD_3$ with a $^{14}N_2$ matrix produced bands between 2274−2266, 1468−1466, and 1463−1460 cm^{-1}. The combination of $(CH_3)_3SiSiD_3$ with a $^{15}N_2$ matrix produced bands at 2198.5 and 2196.5, 1466.6, and 1460.6 cm^{-1}. The combination of $(CH_3)_3SiSiH_3$ with a $^{15}N_2$ matrix produced bands at 2198.5 and 2196.5, 2014.1, and 2010.0 cm^{-1}. These collection of bands were assigned to the N−N stretching, the antisymmetric Si−H stretching, and the symmetric Si−H stretching modes of $H_2Si-{}^{14}N_2$ and its isotopomers $D_2Si-{}^{14}N_2$, $D_2Si-{}^{15}N_2$, and $H_2Si-{}^{15}N_2$.

On the basis of the agreement between our observed bands and those of Maier and co-workers, we assign the bands observed in our experiment to the H_2SiN_2 molecule. Upon initial deposition in the VUV-photolyzed $SiH_4 + {}^{14}N_2$ experiment at 12 K (Figure 2), the band between 2020−2009 cm^{-1} is too broad to observe the antisymmetric and symmetric Si−H stretching modes separately; however, upon annealing the sample to 25 K, distinct bands at 2013.5 and 2009.4 cm^{-1} are observed (parts a and c of Figure 8), and these frequencies are assigned to the antisymmetric and symmetric Si−H stretching modes, respectively, in our experiment. A similar situation is observed in the $SiD_4 + {}^{14}N_2$ experiment (Figure 3), with the antisymmetric and symmetric Si−D stretching bands only becoming clearly distinguishable at 1466.2 and 1458.9 cm^{-1}, respectively, after annealing to 25 K (parts b and d of Figure 8). For the 2275−2266 cm^{-1} bands in the $SiH_4 + {}^{14}N_2$ spectra, four bands at 2274.2, 2272.3, 2270.2, and 2266.3 cm^{-1} are observed upon initial deposition at 12 K, and annealing to 25 K results in retention of the bands at 2274.2 and 2272.3 cm^{-1}, with the 2274.2 cm^{-1} band having the slightly higher intensity. Therefore, the peak at 2274.2 cm^{-1} is assigned to the N−N stretch of H_2SiN_2 in the major trapping site, and the remaining bands are assigned to minor trapping sites. In the $SiD_4 + {}^{15}N_2$ spectra, three bands at 2198.6, 2196.0, and 2191.1 cm^{-1} are observed upon initial deposition at 12 K (Figure 10a), and annealing to 25 K results in retention of the band at 2198.6 cm^{-1} (Figure 10b), which is assigned to the $^{15}N-{}^{15}N$ stretch of $D_2Si^{15}N_2$ in the major trapping site.

The B3LYP/aug-cc-pVTZ calculations predict H_2SiN_2 to be a bent (C_s) molecule with an $^1A'$ ground state (Chart 1), and the unusual nonlinear geometry between the H_2Si and the N_2 appears to due to the presence of a lone pair on the Si atom that is in the H−Si−H plane, causing the N_2 molecule to bind in a nearly perpendicular fashion. The N−N stretching, antisymmetric Si−H stretching, and symmetric Si−H stretching frequencies are predicted to be at 2304.0, 2069.9, and 2062.8 cm^{-1}, respectively, and are found to be in good agreement with the experimentally observed frequencies (deviations of 1.3, 2.7, and 2.6%, respectively) and with the previous calculations performed by Maier and co-workers at the B3LYP/6-311+G**

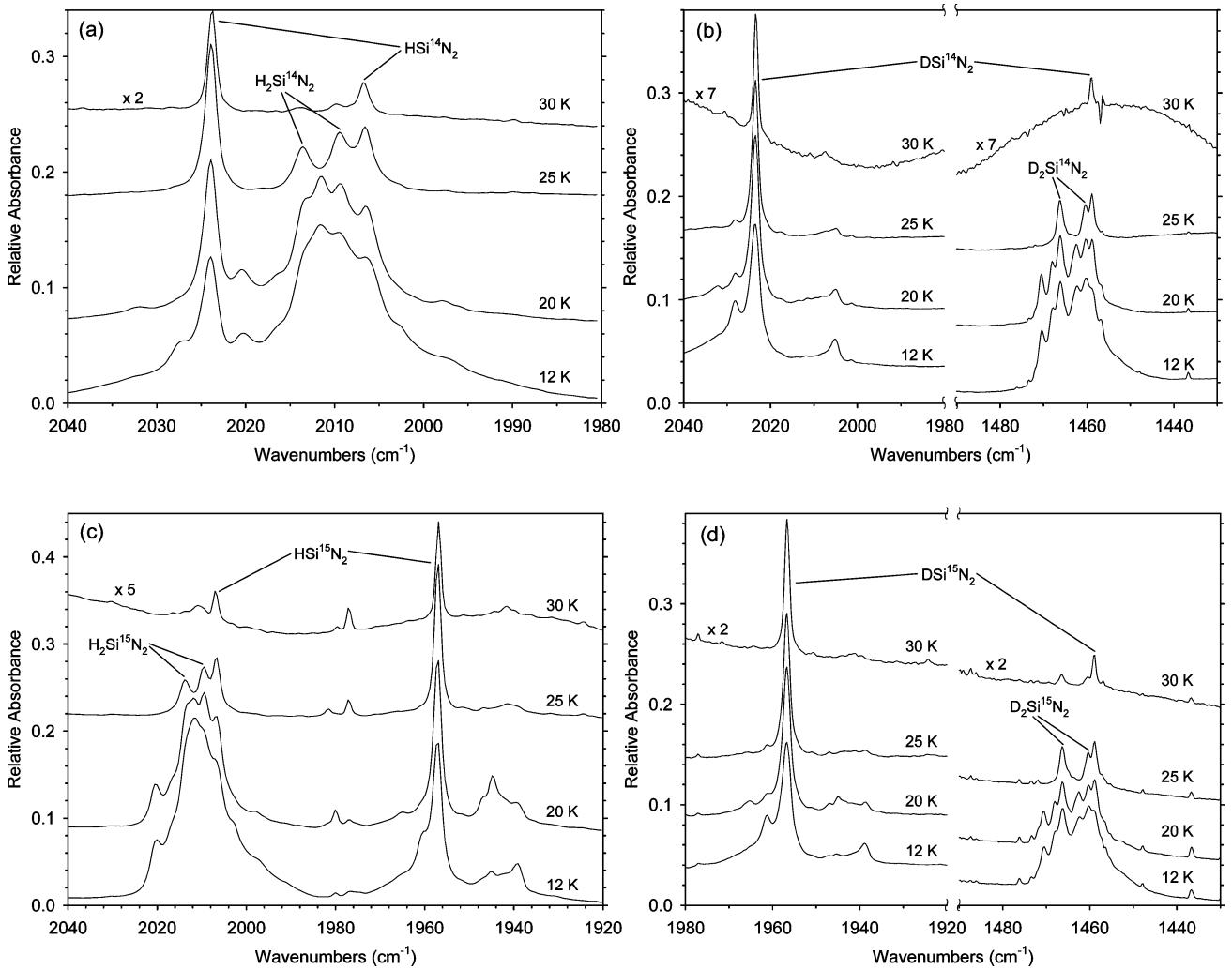

Figure 8. Infrared spectra in the (a) 2040−1980 cm^{-1} region for 1% SiH_4 in $^{14}N_2$, (b) 2040−1980- and 1490−1430 cm^{-1} regions for 1% SiD_4 in $^{14}N_2$, (c) 2040−1920 cm^{-1} region for 1% SiH_4 in $^{15}N_2$, and (d) 2040−1980- and 1490−1430 cm^{-1} regions for 2% SiD_4 in $^{15}N_2$ after 12 K deposition with simultaneous 121.6-nm hydrogen resonance lamp photolysis for 4 h, followed by 20, 25, and 30 K annealing for 30 min at each temperature. For the 30 K annealing experiments, the spectra have been multiplied by the factor indicated.

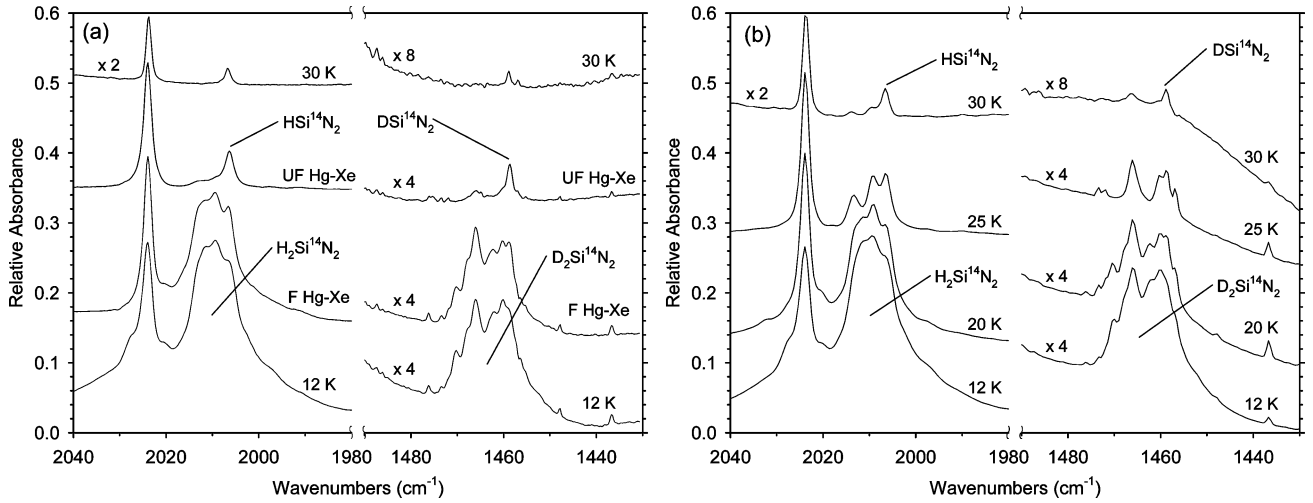

Figure 9. Infrared spectra in the 2040−1980- and 1490−1430 cm^{-1} regions for 0.5% SiH_4 and 0.5% SiD_4 in $^{14}N_2$ after (a) deposition at 12 K with simultaneous 121.6-nm hydrogen resonance lamp photolysis for 4 h (labeled 12 K), followed by 400−900-nm irradiation for 30 min (labeled F Hg−Xe), 200−900-nm irradiation for 30 min (labeled UF Hg−Xe), and annealing to 30 K for 30 min (labeled 30 K) and (b) after 12 K deposition with simultaneous 121.6-nm hydrogen resonance lamp photolysis for 4 h, followed by 20, 25, and 30 K annealing for 30 min at each temperature. Several portions of the spectra have been multiplied by a factor as indicated.

level (2296, 2079, and 2073 cm^{-1}, respectively).[36] With $^{15}N_2$ substitution, the N−N stretching frequency is predicted to shift down by 77.7 cm^{-1} and has a $^{14}N/^{15}N$ ratio of 1.0349. With D_2Si substitution, the antisymmetric and symmetric Si−H stretching frequencies are predicted to shift down by 577.9 and 583.8 cm^{-1}, respectively, and have H/D ratios of 1.3873 and

CHART 1: B3LYP/aug-cc-pVTZ-Optimized Structures (Bond Lengths in Angstroms and Bond Angles in Degrees) of the $HSiN_2$, H_2SiN_2, and H_3SiN_2 Molecules

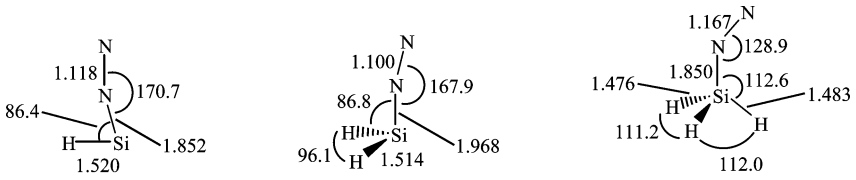

$HSiN_2$; C_s, $^2A''$ H_2SiN_2; C_s, $^1A'$ H_3SiN_2; C_s, $^2A'$

TABLE 2: B3LYP/aug-cc-pVTZ-Calculated Vibrational Frequencies (cm^{-1}) and Intensities (km/mol) of the $HSiN_2$, H_2SiN_2, and H_3SiN_2 Molecules

species	frequency (intensity, symmetry)
$HSiN_2$	2082.6 (608.5,a′), 2042.2 (179.3,a′), 822.8 (32.8,a′), 409.0 (5.1,a′), 319.3 (0.5,a′), 298.2 (1.1,a′)
H_2SiN_2	2304.0 (237.0,a′), 2069.9 (199.1,a″), 2062.8 (126.0,a′), 956.0 (67.7,a′), 747.8 (28.2,a′), 735.9 (9.6,a″), 308.4 (0.1,a′), 272.8 (2.9,a′), 243.3 (1.0,a″)
H_3SiN_2	2272.6 (84.9,a″), 2264.8 (63.4,a′), 2219.6 (68.3,a′), 1877.7 (67.5,a′), 934.1 (59.7,a′), 936.6 (46.4, a″), 905.7 (189.9,a′), 639.5 (58.0,a′), 611.3 (45.1,a″), 489.9 (10.7,a′), 239.8 (0.4,a′), 132.8 (0.2, a″)

1.3947, respectively. The calculations even predict that the antisymmetric and symmetric Si−H stretching frequencies are close to one another, with calculated differences of 7.1 and 13.0 cm^{-1} for H_2SiN_2 and D_2SiN_2, respectively, which is in reasonably good agreement with the experimental values of 4.1 and 7.1 cm^{-1}, respectively. Overall, the calculated isotopic shifts and isotopic ratios are found to be in good agreement with the experimentally observed values, lending support to the assignment of the bands we observe to the H_2SiN_2 molecule. The calculations also predict a SiH_2 bending mode at 956.0 cm^{-1} and a SiH_2 wagging mode at 747.8 cm^{-1} for this molecule, and Maier and co-workers reported observing weak bands at 960.8 and 749.6 cm^{-1} that they assigned to these modes. We looked for bands that could be assigned to these modes; however, we were unable to unambiguously assign any peaks to these modes in our spectra, due to their inherent low intensity and the overlap of this region with the strong SiH_4 and Si_2H_6 vibrations in this region.

With the assignment of the 2013.5 and 2009.4 cm^{-1} bands to the antisymmetric and symmetric Si−H modes of H_2SiN_2, one might expect to observe distinct Si−H and Si−D vibrations in the mixed molecule $HDSiN_2$ and $SiH_4 + SiD_4 + {}^{14}N_2$ experiments were performed in this effort (Figure 9). For $HDSiN_2$, the B3LYP/aug-cc-pVTZ calculations predict the Si−H stretch to be at 2066.1 cm^{-1} and the Si−D stretch at 1485.9 cm^{-1}, which, if compared to the pure isotopic frequencies, puts them in between the pure isotopic antisymmetric and symmetric frequencies. In the mixed $SiH_4 + SiD_4 + {}^{14}N_2$ experiments, we were unable to detect any additional peaks or shoulders that are not already present in the pure isotopic spectra (parts a and b of Figure 8), suggesting that $HDSiN_2$ is not being formed.

The observation of H_2SiN_2 in these experiments represents the second matrix isolation report of this species and by a different route of formation. Therefore, this work provides confirmation of the existence of and proper infrared characterization of the transient H_2SiN_2 molecule.

$HSiN_2$. The sharp band at 2023.9 cm^{-1} (Figure 2) is observed to shift to 1957.1 cm^{-1} with the use of $^{15}N_2$ (Figure 4 and 5) and is not observed to shift with SiD_4 (Figure 3), indicating that this vibration only involves nitrogen. The isotopic $^{14}N/^{15}N$ ratio of this band is found to be 1.0341, suggesting that these bands are due to a N−N stretch of a dinitrogen species. In the mixed $SiH_4 + {}^{14}N_2 + {}^{15}N_2$ and $SiD_4 + {}^{14}N_2 + {}^{15}N_2$ experiments (Figures 6 and 7, respectively), only the pure isotopic counterparts are observed, indicating that only one N_2 subunit is associated with this band. In Figure 2, there is a peak at 2006.6 cm^{-1} that appears after the VUV-photolyzed $SiH_4 + {}^{14}N_2$ sample has been subjected to further photolysis with filtered and unfiltered output of the Hg−Xe lamp (Figure 2c) that initially was thought to be a site peak of the 2023.9 cm^{-1} band; however, it is believed that this is a distinct vibration involving hydrogen and that this mode belongs to the same molecule as the 2023.9 cm^{-1} band. The most convincing evidence for this conclusion comes from a careful analysis of the experiments in which the VUV-photolyzed sample is progressively annealed, and portions of the spectra for these experiments for the $SiH_4 + {}^{14}N_2$, $SiD_4 + {}^{14}N_2$, $SiH_4 + {}^{15}N_2$, and $SiD_4 + {}^{15}N_2$ mixtures are displayed in Figure 8.

As can be seen in parts a and c of Figure 8, after annealing the $SiH_4 + {}^{14}N_2$ and $SiH_4 + {}^{15}N_2$ samples to 25 K, three peaks at 2013.6, 2009.4, and 2006.6 cm^{-1} become clearly distinguishable in the spectra. As discussed above, the 2013.6- and 2009.4 cm^{-1} peaks are assigned to the antisymmetric and symmetric Si−H stretching modes of H_2SiN_2, and the 30 K annealed spectrum shows that the peak at 2006.6 cm^{-1} is distinct from the 2013.6- and 2009.4 cm^{-1} peaks because it is the dominant of the peaks after 30 K annealing. If the 2006.6 cm^{-1} peak was a site splitting of the 2023.9 cm^{-1} band, which is assigned to an N−N stretching mode, then this peak should shift when $^{15}N_2$ is used. However, as can be seen in the $SiH_4 + {}^{15}N_2$ experiment (Figure 8c), after annealing to 25 K the three peaks are still present, and after annealing to 30 K, this band is again the largest peak of the three. The distinct nature of the 2006.6 cm^{-1} peak can also be seen in the unfiltered Hg−Xe photolysis plus 30 K annealing of the $SiH_4 + {}^{15}N_2$ sample (parts c and d of Figure 4), with the 2006.6 cm^{-1} peak clearly still present with the 1957.1 cm^{-1} band after the H_2SiN_2 bands have completely disappeared. That the 2006.6 cm^{-1} band involves hydrogen comes from the SiD_4 experiments (Figures 3 and 5 and parts b and d of Figure 8). In parts b and d of Figure 8, it can be seen that after 25 K annealing three peaks at 1466.2, 1460.4, and 1458.9 cm^{-1} are observed, and after 30 K annealing only the 1458.9 cm^{-1} peak is still present. A similar situation is observed when the SiD_4 samples are subjected to unfiltered Hg−Xe photolysis plus 30 K annealing (Figures 3 and 5), with the 1458.9 cm^{-1} peak being present with the 2023.9 cm^{-1} peak after the D_2SiN_2 bands have disappeared. As it turns out, the 2023.9 cm^{-1} band does have a site splitting band at 2005.1 cm^{-1} (Figures 3 and 8b), which is what led to the initial incorrect

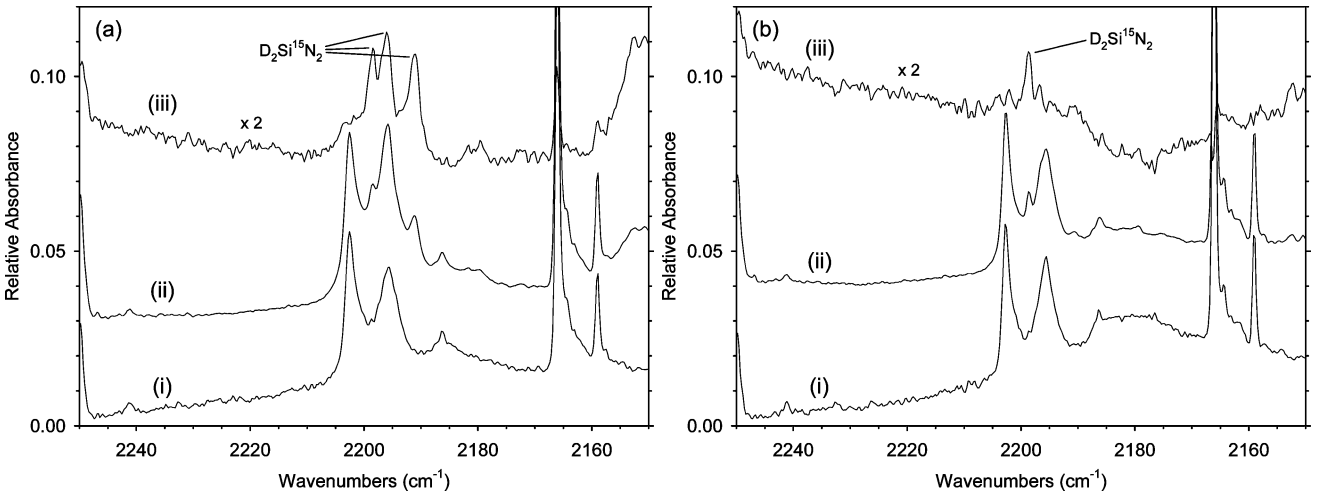

Figure 10. Infrared spectra in the 2250−2150 cm^{-1} region for 2% SiD_4 in $^{15}N_2$ deposited at (a) 12 K and (b) after annealing to 25 K for (i) the deposition of the mixture without hydrogen resonance lamp photolysis and (ii) for the deposition of the mixture with simultaneous hydrogen resonance lamp photolysis. In both parts a and b, the spectrum labeled iii is the result of subtraction of the spectrum labeled i from the spectrum labeled ii, and these subtraction spectra have been multiplied by a factor of 2 as indicated.

assumption that the 2006.6 cm^{-1} peak in the $SiH_4 + {}^{14}N_2$ spectra was a site band; however, the differing Hg−Xe photolysis and annealing behavior of the 2006.6 cm^{-1} band and the 2005.1 cm^{-1} site peak helps to distinguish the two. Once it was realized that the 2006.6 cm^{-1} peak is due to a distinct vibrational mode containing hydrogen, an examination of the spectra in which the 2023.9 and 2006.6 cm^{-1} bands or their $^{15}N_2$ and D counterparts are both present indicated that these bands belong to the same molecule because their relative intensity was approximately the same in the 30 K annealed spectra and in the unfiltered Hg−Xe lamp photolysis spectra. Taking the 1458.9 cm^{-1} as the deuterated counterpart to the 2006.6 cm^{-1} band, the H/D isotopic ratio is found to be 1.3754, which suggests that this band is a Si−H stretching mode. In the mixed $SiH_4 + SiD_4 + {}^{14}N_2$ experiment (Figure 9), only the pure isotopic counterparts are observed, indicating that only one Si−H group is associated with this band.

Having assigned the 2023.9 cm^{-1} band to an N−N stretch and the 2006.6 cm^{-1} band to an Si−H stretch of the same molecule and given the close proximity of the 2006.6 cm^{-1} band to the antisymmetric and symmetric Si−H stretches of H_2SiN_2, a likely candidate seemed to be the $HSiN_2$ molecule, and therefore B3LYP/ aug-cc-pVTZ calculations were performed to determine the optimized geometry and calculated vibrational frequencies for $HSiN_2$. The B3LYP/aug-cc-pVTZ calculations predict $HSiN_2$ to be a bent molecule (C_s) with a $^2A''$ ground state (Chart 1) and similar to H_2SiN_2, the nonlinear geometry between the HSi radical and the N_2 appears to due to the presence of the unpaired electron in an orbital on the Si atom that is collinear with the H−Si axis. The calculated N−N and Si−H stretching frequencies of $HSiN_2$ are predicted to be at 2082.6 and 2042.2 cm^{-1}, respectively, which are 2.8 and 1.7% higher, respectively, supporting the assignments. With $^{15}N_2$ substitution, the N−N stretching frequency is predicted to shift down by 70.3 cm^{-1} and has a calculated $^{14}N/^{15}N$ ratio of 1.0349, which compares favorably with the observed experimental shift (66.3 cm^{-1}) and the observed isotopic ratio (1.0341), again lending support to this assignment. A bending mode of $HSiN_2$ is predicted to lie at 822.8 cm^{-1} and to have an intensity that is predicted to be 5.4% of the intensity of the N−N stretching vibration. A weak band is observed in the $SiH_4 + {}^{14}N_2$ spectra at 813.7 cm^{-1} (1.1% high) that seems to track with the annealing and Hg−Xe photolysis behavior of the 2023.9- and 2006.6 cm^{-1} bands and whose relative intensity with the 2023.9 cm^{-1} band (approximately 4%) is close to the theoretical intensity ratio. In the $SiH_4 + {}^{15}N_2$ spectra, this band is found to be at 810.8 cm^{-1}, and the experimental shift of 2.9 cm^{-1} is similar to the theoretical shift of 3.5 cm^{-1} for the bending frequency of $HSi^{14}N_2$ vs $HSi^{15}N_2$. In the $SiD_4 + {}^{14}N_2$ spectra, we searched for the deuterium counterpart to this bending mode, however; we were unable to unambiguously assign any peak in the appropriate region to this bending mode. In the $SiD_4 + {}^{15}N_2$ spectra a weak band is observed at 627.8 cm^{-1} that seems to track with the annealing and Hg−Xe photolysis behavior of the $^{15}N-{}^{15}N$ and Si−D stretching bands. The experimental shift of 185.9 cm^{-1} from the 813.7 cm^{-1} band for this peak is similar to the theoretical shift of 194.8 cm^{-1} for the bending frequency of $HSi^{14}N_2$ vs $DSi^{15}N_2$, which lends support for the assignment of the 627.8 cm^{-1} band. Also, the experimental intensity ratio of this peak to the $^{15}N-{}^{15}N$ stretching mode in the $SiD_4 + {}^{15}N_2$ spectra (approximately 3%) is similar to the theoretical intensity ratio of 3.2% for the bending mode to the $^{15}N-{}^{15}N$ stretching mode, which again lends support to the assignment.

Ornellas and Iwata have previously studied the theoretical structure and vibrational frequencies of the $HSiN_2$ molecule using the HF, MP2, and CCSD(T) methods and the 6-311G-(2d) basis set.[33] At the HF/6-311G(2d) and MP2/6-311G(2d) levels of theory, the calculations failed to predict a stable, bound complex between the HSi fragment and N_2, whereas the calculations at the CCSD(T)/6-311G(2d) level of theory did predict a bound structure. Similar to the current B3LYP/aug-cc-pVTZ calculations, the CCSD(T)/6-311G(2d) calculations predict the $HSiN_2$ molecule to be a bent molecule with C_s symmetry and an $^2A''$ ground state. At the CCSD(T)/6-311G-(2d) level, the Si−H, Si−N, and N−N bond lengths are predicted to be 1.531, 1.874, and 1.163 Å, respectively, and the HSiN and SiNN angles are predicted to be 86.2 and 171.0°, respectively. As can be seen by comparing the B3LYP/aug-cc-pVTZ calculated bond lengths and bond angles (Chart 1) for $HSiN_2$ to the CCSD(T)/6-311G(2d) calculated values, most seem to be in reasonable agreement, except for the N−N bond length, for which the CCSD(T)/6-311G(2d) calculated value is longer than the B3LYP/aug-cc-pVTZ value by 0.045 Å. Ornellas and Iwata also performed a vibrational frequency analysis for the CCSD(T)/6-311G(2d) optimized $HSiN_2$ structure and reported the SiH stretching, NN stretching, and HSiN bending frequencies

to be 2045, 1690, and 807 cm^{-1}, respectively, at this level. The CCSD(T)/6-311G(2d) calculated SiH stretching and HSiN bending frequencies are found to be in reasonable agreement with the B3LYP/aug-cc-pVTZ-calculated values of 2042.2 and 822.8 cm^{-1}, respectively. However, similar to the disagreement in the calculated N−N bond lengths, the calculated NN stretching frequencies are in disagreement between the two methods, with the B3LYP/aug-cc-pVTZ calculations predicting the NN stretching frequency to occur at 2082.6 cm^{-1}. Given that the experimental NN stretching band has been assigned a value of 2023.9 cm^{-1}, which is close to the B3LYP/aug-cc-pVTZ value, it appears that CCSD(T) method fails to provide a complete and accurate theoretical characterization of the $HSiN_2$ molecule and that the B3LYP method provides a better theoretical characterization of this molecule.

The infrared characterization of the $HSiN_2$ molecule has not been reported previously in the matrix isolation literature, and this work represents the first instance as such. It is worth noting, however, that in their VUV photodissociation experiments with SiH_4 in 12 K nitrogen matrices,[11] Milligan and Jacox did report observing a band at 2026 cm^{-1} that, in hindsight, was most likely the NN stretching band of $HSiN_2$. This would make Milligan and Jacox the first researchers to actually observe a band due to the $HSiN_2$ species; however, as stated previously, they did not fully analyze the nitrogen matrix infrared spectra and therefore never made a definitive assignment for this band.

SiN_2. The bands between 1769−1736 cm^{-1} in the $SiH_4 + {}^{14}N_2$ spectra (Figure 2) are observed to shift to between 1711−1680 cm^{-1} with the use of $^{15}N_2$ (Figure 4) and are not observed to shift with SiD_4 (Figure 3) indicating that this vibration involves nitrogen and does not involve hydrogen. On the basis of the Hg−Xe lamp photolysis and the annealing behavior, the peak at 1754.5 cm^{-1} in the $^{14}N_2$ spectra is assigned to the major trapping site, and the peaks at 1768.1, 1747.9, 1742.8, 1740.4, and 1732.2 cm^{-1} are assigned to minor trapping sites, and the peak at 1697.1 cm^{-1} in the $^{15}N_2$ spectra is assigned to the major trapping site, and the peaks at 1710.6, 1689.6, 1868.0, 1684.9, and 1680.6 cm^{-1} are assigned to minor trapping sites. In the mixed $^{14}N_2 + {}^{15}N_2$ experiments (Figures 6 and 7), only the pure isotopic counterparts are observed indicating that only one N_2 subunit is involved in this mode. The peak at 1754.5 cm^{-1} is in very good agreement with several previously reported experimental matrix isolation assignments of the N−N stretch of linear triplet SiN_2 in nitrogen and argon matrices,[35,44,45] and on the basis of this agreement, we assign the peak at 1754.5 cm^{-1} to triplet SiN_2.

$Si(N_2)_2$. The weak bands between 2048−2042 and 1916−1911 cm^{-1} (Figure 2) are found to shift to 1981−1974 and 1852−1848 cm^{-1}, respectively, with the use of $^{15}N_2$ (Figure 4) and are not found to shift with the use of SiD_4 (Figure 3) indicating that these vibrations involve nitrogen only. On Hg−Xe lamp photolysis and annealing, the intensities of these bands are observed to track with each other, suggesting that these bands belong to different vibrations of the same molecule. In addition, on the basis of the Hg−Xe lamp photolysis and annealing behavior, the peaks at 2044.5 and 1913.0 cm^{-1} in the $^{14}N_2$ spectra are assigned major trapping sites, and the peaks at 2047.9, 2043.3, and 2042.3 cm^{-1} are assigned to minor trapping sites. Similarly, the peaks at 1977.0 and 1849.5 cm^{-1} in the $^{15}N_2$ spectra are assigned major trapping sites, and the peaks at 1852.0, 1850.5, and 1848.4 cm^{-1} are assigned to minor trapping sites. The isotopic $^{14}N/^{15}N$ ratios of the 2044.5−1977.0 cm^{-1} bands and the 1913.0−1849.5 cm^{-1} bands are found to be 1.0341 and 1.0343, respectively, and therefore, these bands are assigned to different N−N stretches in the same molecule. With the assignment of two N_2 subunits being present in this molecule, one expects to observe distinct bands in the mixed $^{14}N_2 + {}^{15}N_2$ experiments (Figures 6 and 7) with frequencies that are in between the pure isotopic counterparts. Unfortunately, due to the low intensities of the $^{14}N_2$ bands at 2048−2042 cm^{-1} and the $^{15}N_2$ bands at 1981−1974 cm^{-1}, distinct mixed isotope bands were not observable in the mixed isotope experiments. In the $SiH_4 + {}^{14}N_2 + {}^{15}N_2$ experiment, the presence of a background peak at 1877.5 cm^{-1} precluded the observation of mixed isotope bands intermediate to the $^{14}N_2$ bands at 1916−1911 cm^{-1} and the $^{15}N_2$ bands at 1852−1848 cm^{-1}; however, in the $SiD_4 + {}^{14}N_2 + {}^{15}N_2$ experiment, two weak bands were observed at 1875.9 and 1870.9 cm^{-1}, supporting the assignment of two N_2 subunits being present in the molecule.

In a study in which vaporized silicon was deposited with nitrogen at 12 K, Maier and co-workers[35] observed bands at 2045.0 and 1912.9 cm^{-1} that they assigned to the symmetric and antisymmetric N−N stretching modes, respectively, of $Si(N_2)_2$. When $^{15}N_2$ was used these bands were found to shift to 1977.0 and 1849.4 cm^{-1}, respectively. On the basis of the agreement between the bands we observed in our experiments and those reported by Maier and co-workers, we assign the weak bands at 2044.5 and 1913.0 cm^{-1} observed in our experiment to the symmetric and antisymmetric N−N stretching modes of the $Si(N_2)_2$ molecule.

Additional Possible Spectroscopic Candidates. With the observation of the $HSiN_2$ and H_2SiN_2 species, we looked for infrared bands that could be attributed to SiH_3 or H_3SiN_2. To search for "free" SiH_3, we used the observed SiH_3 frequencies of Andrews and Wang at 928.6, 735.4, and 727.3 cm^{-1} in a 3.5 K neon matrix[15] as a guide; however, we were unable to unambiguously assign any peaks in these regions to "free" SiH_3. To search for peaks that could be assigned to H_3SiN_2, we performed B3LYP/aug-cc-pVTZ calculations and found a bound minimum for this molecule, which has a bent structure (C_s) with a $^2A'$ ground state (Chart 1) and vibrational frequencies that are listed in Table 2. By use of these frequencies as a guide, we were unable to assign a set of peaks that could be attributed exclusively to the H_3SiN_2 molecule. It is interesting to note that the dissociation of H_3SiN_2 into H_3Si and N_2 is predicted to be exothermic by 44.1 kJ/mol, and the only reason a bound minimum is obtained for the calculation is due to a barrier to dissociation of approximately 28 kJ/mol, which was found by performing a rigid potential energy scan along the Si−N bond stretching coordinate from the minimized structure.

Trend in X−N_2 Stretching Frequencies. With the observation of three species involving the complexation of a single nitrogen molecule (SiN_2, $HSiN_2$, and H_2SiN_2) and coupling that with the vibrational frequency of a "free" N_2 in a nitrogen matrix (2328.1 cm^{-1}),[16] a trend in the N−N stretching frequencies is now evident. As can be seen for Table 1, the N−N stretching frequencies decrease in the order $N_2 > H_2SiN_2 > HSiN_2 > SiN_2$. Since the number of unpaired electrons on the silicon atom is 0, 1, and 2 in H_2SiN_2, $HSiN_2$, and SiN_2, respectively, the decrease in the N−N stretching frequency most likely reflects an increased amount of back-bonding from the silicon atom to a π^* orbital on the nitrogen molecule as the number of unpaired electrons increases. The increased back-bonding leads to a weakening of the N−N bond strength and therefore a decreasing of the N−N stretching frequency. This increased back-bonding is also evidenced by the N−N bond lengths, which increase in the order N_2 (1.091 Å, calculated value) < H_2SiN_2 < $HSiN_2$ < SiN_2 (1.141 Å, calculated value).

Formation Energetics. On the basis of products observed in the current nitrogen matrix experiments (SiN_2, $HSiN_2$, H_2SiN_2, Si_2H_2, and Si_2H_6), some indications of the overall reaction pathways to produce these products can be inferred. The hydrogen resonance lamp used in these experiments produce radiation with a wavelength of 121.6 nm (983.7 kJ.mol), and from gas-phase photoabsorption and photodissociation experiments with SiH_4,[6−8] this is thought to excite SiH_4 to a dissociative singlet Rydberg state. Since the complexes of a nitrogen molecule with SiH_2, SiH, and Si atoms are observed in our experiments, this implies that SiH_2, SiH, and Si atoms are formed from the dissociation of SiH_4. Several ab initio studies of the SiH_4 singlet excited-state potential energy surfaces have demonstrated that reaction pathways exist that connect the excited states of SiH_4 that are accessible with VUV irradiation to either excited states or the ground states of the SiH_2, SiH, and Si products.[46−50] In the cases where an excited state of one of these products is initially formed, the excited species is most likely relaxed to the ground state by collisions with the nitrogen matrix. It was also found by ab initio calculations that the formation of SiH_3 (and a hydrogen atom) does not occur directly from the excited singlet state surfaces of SiH_4, and this probably accounts for why SiH_3 is not observed in our experiments.[51] To simplify the discussion of the formation energetics, generally only the ground-state reaction pathways will be considered below, and these reaction energies have been calculated at the B3LYP/aug-cc-pVTZ level (corrected for zero-point energies). For the details of the excited-state pathways of SiH_4 that lead to the SiH_2, SiH, and Si products, the reader is referred to the previous ab initio studies and references therein.[46−50]

The energetics for the most direct routes for forming SiH_2, SiH, and Si atoms from SiH_4 are listed in reactions 1−3

$$SiH_4\ (^1A_1) \rightarrow SiH_2\ (^1A_1) + H_2\ (^1\Sigma_g^+) \qquad \Delta E = 221.5\ \text{kJ/mol} \quad (1)$$

$$SiH_4\ (^1A_1) \rightarrow SiH\ (^2\Pi) + H_2\ (^1\Sigma_g^+) + H\ (^2S) \qquad \Delta E = 530.9\ \text{kJ/mol} \quad (2)$$

$$SiH_4\ (^1A_1) \rightarrow Si\ (^3P) + 2H_2\ (^1\Sigma_g^+) \qquad \Delta E = 396.0\ \text{kJ/mol} \quad (3)$$

Of these reactions, reaction 3 is unlikely to occur as a direct reaction because the formation of a triplet silicon atom from a singlet SiH_4 will be spin forbidden. More likely the silicon atom is formed in a singlet excited-state followed by relaxation to the triplet state silicon atom and the energetics of the dissociation of SiH_4 into Si (^{1}D) is given in reaction 4

$$SiH_4\ (^1A_1) \rightarrow Si\ (^1D) + 2H_2\ (^1\Sigma_g^+) \qquad \Delta E = 501.6\ \text{kJ/mol} \quad (4)$$

It is also possible that reactions 1, 2, and 4 involve primarily or additional hydrogen atoms as products and the energetics of these alternatives is given in reactions 5−7

$$SiH_4\ (^1A_1) \rightarrow SiH_2\ (^1A_1) + 2H\ (^2S) \qquad \Delta E = 655.7\ \text{kJ/mol} \quad (5)$$

$$SiH_4\ (^1A_1) \rightarrow SiH\ (^2\Pi) + 3H\ (^2S) \qquad \Delta E = 965.1\ \text{kJ/mol} \quad (6)$$

$$SiH_4\ (^1A_1) \rightarrow Si\ (^1D) + H_2\ (^1\Sigma_g^+) + 2H(^2S) \qquad \Delta E = 935.8\ \text{kJ/mol} \quad (7)$$

The production of all hydrogen atoms in reactions 4 is calculated to be 1370.0 kJ/mol, which is above the excitation energy and therefore not a possibility.

Since the SiH_2 and SiH fragments may be formed with considerable excess excitation energy still in the molecule, it is also possible that once formed they dissociate further, and the simplest, decomposition reactions involving SiH_2 and SiH are given as reactions 8−10

$$SiH_2\ (^1A_1) \rightarrow SiH\ (^2\Pi) + H\ (^2S) \qquad \Delta E = 309.3\ \text{kJ/mol} \quad (8)$$

$$SiH\ (^2\Pi) \rightarrow Si\ (^3P) + H\ (^2S) \qquad \Delta E = 299.3\ \text{kJ/mol} \quad (9)$$

$$SiH\ (^2\Pi) \rightarrow Si\ (^1D) + H\ (^2S) \qquad \Delta E = 416.9\ \text{kJ/mol} \quad (10)$$

It is worth noting that reactions 9 and 10 would only be possible if SiH is formed from reaction 2, with H_2 as the coproduct.

It is difficult to say with certainty from our experiments whether reactions 1, 2, and 4, which involve molecular hydrogen, or reactions 5−7, which involve significant amounts of hydrogen atoms, are the dominant formation reactions or whether the secondary dissociation reactions 8−10 lead to considerable amounts of the SiH_x fragments. However, if a considerable amount of hydrogen atoms were present in the matrix, one might expect the formation of a considerable concentration of the mixed $HDSiN_2$ isotopomer in the $SiH_4 + SiD_4 + {}^{14}N_2$ experiments resulting from the reverse of reaction 8. The lack of the observation of the $HDSiN_2$ isotopomer seems to indicate that reactions involving molecular hydrogen are dominant. Once the ground-state species Si, SiH, and SiH_2 are formed in the 12 K nitrogen matrix, each of these fragments complexes with a nitrogen molecule via an exothermic reaction to yield the SiN_2, $HSiN_2$, and H_2SiN_2 species, which are given in reactions 11−13

$$Si\ (^3P) + N_2\ (^1\Sigma_g^+) \rightarrow SiN_2\ (^3\Sigma^-) \qquad \Delta E = -72.5\ \text{kJ/mol} \quad (11)$$

$$SiH\ (^2\Pi) + N_2\ (^1\Sigma_g^+) \rightarrow HSiN_2\ (^2A'') \qquad \Delta E = -46.3\ \text{kJ/mol} \quad (12)$$

$$SiH_2\ (^1A_1) + N_2\ (^1\Sigma_g^+) \rightarrow H_2SiN_2\ (^1A') \qquad \Delta E = -25.2\ \text{kJ/mol} \quad (13)$$

The relative energetics of reactions 11−13 generally appear to be reflected in the annealing behavior of SiN_2, $HSiN_2$, and H_2SiN_2 in that the bands due to H_2SiN_2 disappear first and at the lowest temperatures upon annealing, followed by the bands of $HSiN_2$, and then finally the bands of SiN_2 (Figures 1S−4S). Since the $Si(N_2)_2$ molecule is observed in our experiments, some of the SiN_2 formed from reaction 11 reacts further with a second N_2, and this is given in reaction 14

$$SiN_2\ (^3\Sigma^-) + N_2\ (^1\Sigma_g^+) \rightarrow Si(N_2)_2\ (^1A_1) \qquad \Delta E = +27.5\ \text{kJ/mol} \quad (14)$$

Although, reaction 14 is predicted to be endothermic, the overall formation from Si (^{3}P) is predicted to be exothermic (−45.0

kJ/mol). It is also possible that the $Si(N_2)_2$ is being formed from stepwise reactions of Si (^1D) and SiN_2 ($^1\Sigma^+$) with N_2, and these are given in reactions 15 and 16

$$Si\ (^1D) + N_2\ (^1\Sigma_g^+) \rightarrow SiN_2\ (^1\Sigma^+) \qquad \Delta E = -98.0\ \text{kJ/mol} \quad (15)$$

$$SiN_2\ (^1\Sigma^+) + N_2\ (^1\Sigma_g^+) \rightarrow Si(N_2)_2\ (^1A_1) \qquad \Delta E = -52.6\ \text{kJ/mol} \quad (16)$$

Secondary reactions of the SiH_x fragments most likely lead to the Si_2H_2 and Si_2H_6 species, and the simplest of these reactions are listed in reactions 17 and 18

$$SiH\ (^2\Pi) + SiH\ (^2\Pi) \rightarrow Si_2H_2\ (^1A_1) \qquad \Delta E = -308.7\ \text{kJ/mol} \quad (17)$$

$$SiH_2\ (^1A_1) + SiH_4\ (^1A_1) \rightarrow Si_2H_6\ (^1A_{1g}) \qquad \Delta E = -205.3\ \text{kJ/mol} \quad (18)$$

Conclusion

VUV photolysis (121.6 nm) of silane in a nitrogen matrix at 12 K leads to the observation of several transient species, which have been characterized using Fourier transform infrared spectroscopy. Four transient species containing silicon and nitrogen have been observed (SiN_2, $Si(N_2)_2$, $HSiN_2$, and H_2SiN_2), and one species only containing silicon and hydrogen has been observed (Si_2H_2). The identification and assignment of the infrared bands due to each of these species was accomplished by performing isotopic substitution experiments (SiD_4, $^{15}N_2$, and mixtures with SiH_4 and $^{14}N_2$), matrix annealing experiments, UV−vis photolysis experiments, by comparison with previous experimental matrix isolation frequencies, where available, and for $HSiN_2$ and H_2SiN_2 by comparison to B3LYP/aug-cc-pVTZ-calculated vibrational frequencies. The observation and infrared assignment of the $HSiN_2$ and H_2SiN_2 molecules in these experiments is significant, in that $HSiN_2$ has not been previously reported in the matrix isolation literature, and H_2SiN_2 has only been reported once previously by a different route of formation. The energetics of the overal formation pathways for each of these molecules is discussed using B3LYP/aug-cc-pVTZ calculations.

Acknowledgment. Acknowledgment is made to Penn State Erie (start-up funds and Early Career Faculty Research Incentive Grant), Research Corporation (Cottrell College Science Award # CC5904), and the Donors of the American Chemical Society Petroleum Research Fund (Type G Grant No. 43110-GB5) for support of this research. C.T.D., D.G.I., C.J.L., N.C.R., and N.L.S. also acknowledge Penn State Erie for support in the form of Undergraduate Research Fellowship Awards.

Supporting Information Available: Infrared spectra for the 12 K hydrogen lamp photolysis experiments followed by the progressive 20, 25, and 30 K annealing experiments for each of the mixtures described in the text. This material is available free of charge via the Internet at http://pubs.acs.org.

References and Notes

(1) *Thin Film Processes*; Vossen, J. L., Kern, W., Eds.; Academic Press: New York, 1978; pp 257−331.
(2) *Chemical Vapor Deposition: Principles and Applications*; Hitchman, M. L., Jensen, K. F., Eds.; Academic Press: San Diego, 1993.
(3) *CVD of Nonmetals*; Rees, W. S., Jr., Ed.; VCH: New York, 1996.
(4) Eden, J. G. *Photochemical Vapor Deposition*; John Wiley & Sons: New York, 1992.
(5) Washida, N.; Matsumi, Y.; Hayashi, T.; Ibuki, T.; Hiraya, A.; Shobatake, K. *J. Chem. Phys.* **1985**, *83*, 2769.
(6) Suto, M.; Lee, L. C. *J. Chem. Phys.* **1986**, *84*, 1160.
(7) Itoh, U.; Toyoshima, Y.; Onuki, H.; Washida, W.; Ibuki, I. *J. Chem. Phys.* **1986**, *85*, 4867.
(8) Glenewinkel-Meyer, T.; Bartz, J. A.; Thorson, G. M.; Crim, F. F. *J. Chem. Phys.* **1993**, *99*, 5944.
(9) Henck, R.; Fuchs, C.; Fogarassy, E. *J. Appl. Phys.* **1996**, *79*, 2259.
(10) Jasinski, J. M.; Meyerson, B. S.; Scott, B. A. *Ann. Rev. Phys. Chem.* **1987**, *38*, 109.
(11) Milligan, D. E.; Jacox, M. E. *J. Chem. Phys.* **1970**, *52*, 2594.
(12) Fredin, L.; Hauge, R. H.; Kafafi, Z. H.; Margrave, J. L. *J. Chem. Phys.* **1985**, *82*, 3542.
(13) Lloret, A.; Abouaf-Marguin, L. *Chem. Phys.* **1986**, *107*, 139.
(14) Li, L.; Graham, J. T.; Weltner, W. *J. Phys. Chem. A* **2001**, *105*, 11018.
(15) Andrews, L.; Wang, X. *J. Phys. Chem. A* **2002**, *106*, 7696.
(16) Amicangelo, J. C.; Collier, J. R.; Dine, C. T.; Saxton, N. S.; Schleicher, R. M. *Mol. Phys.* **2007**, *105*, 989.
(17) Fehsenfeld, F. C.; Evenson, K. M.; Broida, H. P. *Rev. Sci. Instrum.* **1965**, *36*, 294.
(18) Becke, A. D. *J. Chem. Phys.* **1993**, *98*, 5648.
(19) Lee, C.; Yang, W.; Parr, R. G. *Phys. Rev. B* **1988**, *37*, 785.
(20) Dunning, T. H. *J. Chem. Phys.* **1989**, *90*, 1007.
(21) Kendall, R. A.; Dunning, T. H.; Harrison, R. J. *J. Chem. Phys.* **1992**, *96*, 6796.
(22) Woon, D. E.; Dunning, T. H. *J. Chem. Phys.* **1993**, *98*, 1358.
(23) Frisch, M. J.; Trucks, G. W.; Schlegel, H. B.; Scuseria, G. E.; Robb, M. A.; Cheeseman, J. R.; Montgomery, J. A., Jr.; Vreven, T.; Kudin, K. N.; Burant, J. C.; Millam, J. M.; Iyengar, S. S.; Tomasi, J.; Barone, V.; Mennucci, B.; Cossi, M.; Scalmani, G.; Rega, N.; Petersson, G. A.; Nakatsuji, H.; Hada, M.; Ehara, M.; Toyota, K.; Fukuda, R.; Hasegawa, J.; Ishida, M.; Nakajima, T.; Honda, Y.; Kitao, O.; Nakai, H.; Klene, M.; Li, X.; Knox, J. E.; Hratchian, H. P.; Cross, J. B.; Bakken, V.; Adamo, C.; Jaramillo, J.; Gomperts, R.; Stratmann, R. E.; Yazyev, O.; Austin, A. J.; Cammi, R.; Pomelli, C.; Ochterski, J. W.; Ayala, P. Y.; Morokuma, K.; Voth, G. A.; Salvador, P.; Dannenberg, J. J.; Zakrzewski, V. G.; Dapprich, S.; Daniels, A. D.; Strain, M. C.; Farkas, O.; Malick, D. K.; Rabuck, A. D.; Raghavachari, K.; Foresman, J. B.; Ortiz, J. V.; Cui, Q.; Baboul, A. G.; Clifford, S.; Cioslowski, J.; Stefanov, B. B.; Liu, G.; Liashenko, A.; Piskorz, P.; Komaromi, I.; Martin, R. L.; Fox, D. J.; Keith, T.; Al-Laham, M. A.; Peng, C. Y.; Nanayakkara, A.; Challacombe, M.; Gill, P. M. W.; Johnson, B.; Chen, W.; Wong, M. W.; Gonzalez, C.; Pople, J. A. *Gaussian 03*, revision D.01; Gaussian, Inc.: Wallingford, CT, 2004.
(24) Maier, G.; Reisenauer, H. P.; Meudt, A.; Egenolf, H. *Chem. Ber.* **1997**, *130*, 1043.
(25) Maier, G.; Reisenauer, H. P.; Glatthaar, J. *Chem.−Eur. J.* **2002**, *8*, 4383.
(26) DeKock, R. L.; Grev, R. S.; III, H. F. S. *J. Chem. Phys.* **1988**, *89*, 3016.
(27) Cai, Z. L.; Wang, Y. F.; Xiao, H. M. *J. Chem. Soc., Faraday Trans.* **1992**, *88*, 1611.
(28) Murray, C. W.; Laming, G. J.; Handy, N. C.; Amos, R. D. *J. Phys. Chem.* **1993**, *1993*, 1868.
(29) Huhn, M. M.; Amos, R. D.; Kobayashi, R.; Handy, N. C. *J. Chem. Phys.* **1993**, *98*, 7107.
(30) Wang, J.; Eriksson, L. A.; Boyd, R. J.; Shi, Z.; Johnson, B. G. *J. Phys. Chem.* **1994**, *98*, 1844.
(31) Davy, R. D.; Schaefer, H. F., III *Chem. Phys. Lett.* **1996**, *255*, 171.
(32) Ornellas, F. R.; Ueno, L. T.; Iwata, S. *J. Chem. Phys.* **1997**, *106*, 151.
(33) Ornellas, F. R.; Iwata, S. *Bull. Chem. Soc. Japan* **1997**, *70*, 2057.
(34) Pak, C.; Rienstra-Kiracofe, J. C.; Schaefer, H. F. *J. Phys. Chem. A* **2000**, *104*, 11232.
(35) Maier, G.; Reisenauer, H. P.; Glatthaar, J. *Organometallics* **2000**, *19*, 4775.
(36) Maier, G.; Reisenauer, H. P.; Glatthaar, J.; Zetzmann, R. *Chem. Asian J.* **2006**, *1−2*, 195.
(37) Tsuzuki, S.; Honda, K.; Uchimaru, T.; Mikami, M.; Tanabe, K. *J. Am. Chem. Soc.* **2000**, *122*, 11450.
(38) Sinnokrot, M. O.; Valeev, E. F.; Sherrill, C. D. *J. Am. Chem. Soc.* **2002**, *124*, 10887.
(39) Sinnokrot, M. O.; Sherrill, C. D. *J. Phys. Chem. A* **2004**, *108*, 10200.
(40) Sinnokrot, M. O.; Sherrill, C. D. *J. Am. Chem. Soc.* **2004**, *126*, 7690.
(41) Lee, E. C.; Hong, B. H.; Lee, J. Y.; Kim, J. C.; Kim, D.; Kim, Y.; Tarakeshwar, P.; Kim, K. S. *J. Am. Chem. Soc.* **2005**, *127*, 4530.
(42) Tsuzuki, S.; Uchimaru, T.; Mikami, M. *J. Phys. Chem. A* **2006**, *110*, 2027.
(43) Park, Y. C.; Lee, J. S. *J. Phys. Chem. A* **2006**, *110*, 5091.

(44) Lembke, R. R.; Ferrante, R. F.; Weltner, W. *J. Am. Chem. Soc*. **1977**, *99*, 416.
(45) Meloni, G.; Cesaro, S. N.; Sanna, N. *Chem. Phys. Lett*. **2001**, *343*, 113.
(46) Gordon, M. S.; *Chem. Phys. Lett.* **1980**, *70*, 343.
(47) Oikawa, S.; Tsuda, M.; Yoshida, J.; Jisai, Y. *J Chem. Phys.* **1986**, *85*, 2808.
(48) Francisco, J. S.; Barnes, R.; Thoman, J. W. *J Chem. Phys.* **1988**, *88*, 2334.
(49) Tsuda, M.; Oikawa, S.; Sato, K. *J Chem. Phys.* **1989**, *91*, 6822.
(50) Chantranupong, L.; Hirsch, G.; Buenker, R. J. *Chem. Phys.* **1993**, *170*, 167.
(51) Tsuda, M.; Oikawa, S.; Nagayama, K. *Chem. Phys. Lett*. **1985**, *118*, 498.